https://doi.org/10.5194/egusphere-2024-2927
Preprint. Discussion started: 17 October 2024

Calving from horizontal forces in a revised crevasse-depth framework

Donald A. Slater[1] and Till J. W Wagner[2]

[1]School of Geosciences, University of Edinburgh
[2]Atmospheric and Oceanic Sciences, University of Wisconsin Madison

Correspondence: Donald A. Slater (donald.slater@ed.ac.uk)

Abstract. Calving is a key process for the future of our ice sheets and oceans, but representing it in models remains challenging. Among numerous possible calving parameterisations, the crevasse-depth law remains attractive for its clear physical interpretation and its performance in models. In its classic form, however, it requires ad-hoc and arguably unphysical modifications to produce crevasses that are deep enough to result in calving. Here, we adopt a recent analytical approach accounting for the feedback between crevassing and the stress field and varying the density of water in basal crevasses, and show that it removes the need for such ad-hoc modifications. After accounting for ice tensile strength and basal friction, we show that the revised formulation predicts that full-thickness calving should occur at flotation when the calving front ice thickness is greater than around 400 m. It also predicts no calving for ice thinner than around 400 m, suggesting that calving at such glacier fronts is not driven purely by horizontal forces. We find good observational support for this analysis. We advance the revised crevasse-depth formulation as a step towards understanding differing calving styles and a better representation of calving in numerical models.

1 Introduction

Glacier and ice shelf calving plays an important role in our climate system. This is most prominently due to its influence on mass loss from bodies of ice and thereby sea-level rise (Fox-Kemper, 2021), but also due to the climate and ecosystem effects of iceberg melting over the polar ocean (see review by Alley et al., 2023). Beyond its significance in the physical world, calving takes on an outsized role in climate modelling as it presents a crucial boundary condition linking ice sheet and ocean models (Benn et al., 2017; Alley et al., 2023).

Calving is a complex phenomenon that varies in character in both space and time (e.g., Benn et al., 2007; Bassis and Jacobs, 2013) and is influenced by surface melting (Cook et al., 2012), wave action (Petlicki et al., 2015), tides (Holmes et al., 2023), submarine melting (Luckman et al., 2015) and buttressing by mélange and sea ice (Miles et al., 2017; Wehrlé et al., 2023). In Greenland, most calving occurs at the front of grounded tidewater glaciers. It can be characterised as consisting of either (i) low volume but high frequency events, sometimes generally called serac failure (e.g., How et al., 2019); or (ii) high volume but low frequency, full-thickness events (e.g., James et al., 2014), though there are other ways of characterising calving styles and a continuum of possibilities may be more realistic (e.g., Alley et al., 2023). Full-thickness calving tends to be more common for

https://doi.org/10.5194/egusphere-2024-2927
Preprint. Discussion started: 17 October 2024

glacier termini that are close to or at flotation, and in particular is the style of calving that leads to the loss of tabular icebergs from Antarctica's ice shelves. At the level of the stresses experienced by the ice, calving can be driven by horizontal (van der Veen, 1998; Todd et al., 2018), vertical (Ma et al., 2017; Slater et al., 2021) and rotational forces (Wagner et al., 2016; Sartore et al., 2024), or perhaps by any combination of the three (Bassis and Walker, 2012; Ma and Bassis, 2019; Cowton et al., 2019; Schlemm and Levermann, 2019).

The search for better fundamental understanding of the calving process has seen the use of damage and linear elastic fracture mechanics approaches to investigate the nucleation and propagation of ice cracks (Duddu et al., 2013; Albrecht and Levermann, 2014; Yu et al., 2017; Lai et al., 2020; Zarrinderakht et al., 2022; Gao et al., 2023). Complementary to this, modeling approaches that treat glaciers as a large number of discrete ice "particles" allow a range of calving behaviours to emerge as a result of the modeled stresses and the breaking of bonds between the particles (Bassis and Jacobs, 2013; Åström et al., 2014; van Dongen et al., 2020). High-resolution, three-dimensional continuum modeling gives detailed insight into stresses within the ice and – after adoption of a calving criterion – suggests how calving may respond to geometry and environmental forcings (e.g., Todd et al., 2018; Holmes et al., 2023).

Without further parameterisation of their results, however, such approaches are not realistically implementable as calving conditions in large-scale ice sheet models, such as the continent-scale simulations run as part of the Ice Sheet Model Intercomparison Project (ISMIP6; Goelzer et al., 2020; Seroussi et al., 2020). The challenge in formulating such calving conditions is to find a unifying criterion that is general enough to capture the dominant calving behavior for a wide variety of physical settings yet simple enough to be represented in continuum models that may struggle for resolution at the marine boundary and may not solve for all components of the stress tensor. In particular, to render long-term continent-scale simulations computationally feasible, most models are simplified to a depth-integrated framework. As a result, a calving law that draws solely on depth-integrated quantities is highly sought after.

Many such depth-integrated calving laws have been proposed, often grouped into "rate" and "position" laws (Amaral et al., 2020), though there is a close relationship between these groups. Rate laws conceptualise calving as a process that removes mass from the calving front at a given rate and thus characteristically consider strain rates and flow velocities (e.g., Levermann et al., 2012; Morlighem et al., 2016; Mercenier et al., 2018). Position laws conceptualise calving as a process that removes ice to a given position upstream from the terminus and characteristically consider geometry and stress thresholds (e.g., Van der Veen, 1996, 2002; Pfeffer et al., 1997; Benn et al., 2007). The approach used in this study – the relation between modeled crevasse penetration depths and calving – is an example of a position law.

Nye (1955) laid the foundation of how stress balances in the ice sheet could be applied to estimate maximum stable surface crevasse depths. Weertman (1973) added hydrofracture – the deepening of surface crevasses due to the presence of meltwater – while Jezek (1984) applied a similar framework to basal crevasses. Benn et al. (2007) linked crevasse depths to the calving process, suggesting that calving could be assumed to occur when the surface crevasses reached the sea surface waterline (rather than requiring full-depth penetration). This concept was developed further by Nick et al. (2010), who also accounted for the potential presence of basal crevasses and took calving to occur when surface and basal crevasses meet. Versions of the law

https://doi.org/10.5194/egusphere-2024-2927
Preprint. Discussion started: 17 October 2024

developed by Nick et al. (2010) have been widely used since (e.g., Nick et al., 2013; Todd et al., 2019; Cook et al., 2022; Holmes et al., 2023).

Rate and position calving laws have been compared and validated against observations. On the one hand, Choi et al. (2018) and Wilner et al. (2023) conclude that rate calving laws result in the closest matches between modeled and observed calving front position for specific Greenland glaciers and Antarctic ice shelves, respectively. On the other hand, based purely on observations, Amaral et al. (2020) argue that the crevasse-depth law of Nick et al. (2010) is generally highly accurate. They find this law to be relatively insensitive to imperfect parameter calibration, so that a single parameter value can readily be applied to many glaciers, while rate laws require more glacier-specific tuning. The crevasse-depth approach thus remains a leading contender for a high-fidelity, low-complexity calving parameterisation.

Despite this conclusion, the crevasse-depth law remains hamstrung by the fact that in its basic formulation, the modeled crevasse depths close to the calving front are not deep enough to drive calving. This has led to understandable but unsatisfactory modifications, such as the proposal that calving occurs when surface crevasses reach the sea surface (Benn et al., 2007), without detailed physical consideration of how the remaining ice fractures, or the use of meltwater as a tuning parameter to deepen surface crevasses, with little observational evidence linking the presence of meltwater in surface crevasses to calving (Amaral et al., 2020; Enderlin and Bartholomaus, 2020).

Here, we revisit the original crevasse-depth law, but account for the feedback between crevasses and the stress field, and for variable density of water in basal crevasses, with an approach recently employed by Buck (2023) in the context of ice shelf rifting. We adapt the approach to grounded tidewater glaciers and extend it by considering ice tensile strength and basal friction. We find that these modifications generally lead to significantly larger crevasses and can give full-depth crevassing without appealing to water in surface crevasses. Furthermore, the resulting "modified" crevasse-depth law has interesting properties that show promise at explaining differing calving styles. This paper proceeds by first presenting the original crevasse-depth law, then the modification, then the results – predicted crevasse sizes and the sensitivity to physical parameters, the modified calving criterion and the possible role of basal friction. We discuss observational support for the findings and conclude by placing the findings in the context of the ongoing search for better calving parameterisations.

2 Methods

2.1 Set-up

We consider a flow-line marine-terminating glacier with calving front at $x = x_{cf}$, sea level at $z = 0$ and constant ice density ρ_i (Fig. 1). The bed topography in the marine-based part of the glacier is $z = -w(x)$ so that the ocean depth at the calving front is $w(x_{cf})$. The ice thickness is $H(x)$, giving an ice surface elevation above sea level $h(x) = -w(x) + H(x)$. It is assumed there is an open hydraulic connection from the bed below the glacier to the calving front, so that where the bed is below sea level, the water pressure at the base of the glacier is $\rho_w g w(x)$, with density of seawater ρ_w and gravitational acceleration g. The depth of surface crevasses is denoted $d_s(x)$ and the height of basal crevasses is $d_b(x)$; when referring to both surface and basal crevasses we use 'size' rather than 'depth' or 'height'. Surface crevasses are assumed to be dry and basal crevasses are

https://doi.org/10.5194/egusphere-2024-2927
Preprint. Discussion started: 17 October 2024

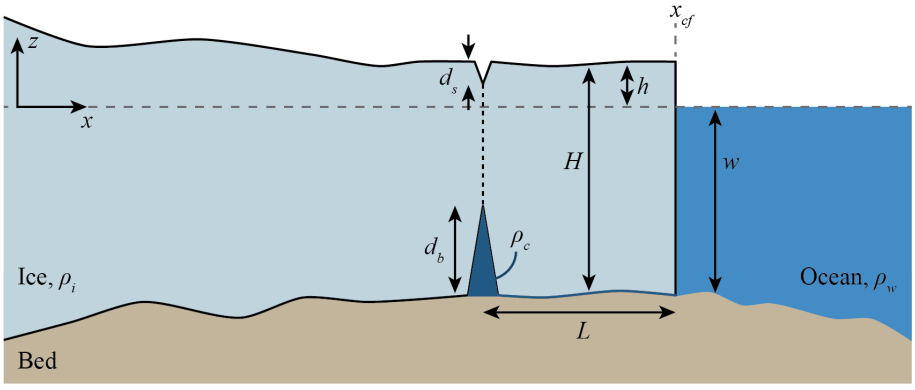

Figure 1. Schematic of a grounded marine-terminating glacier, having thickness $H(x)$ and density ρ_i. Indicated are the ocean water depth $w(x)$, height of ice surface above sea level $h(x)$, surface crevasse penetration depth d_s, and basal crevasse height d_b. Ocean water has density ρ_w and water in the basal crevasse has density ρ_c. The horizontal distance between the crevasse pair and the calving front x_{cf} is L.

assumed to be filled with water of density ρ_c. For the numerical results in this paper, we take $g = 9.81\ \mathrm{m\,s^{-2}}$, $\rho_i = 917\ \mathrm{kg\,m^{-3}}$ and $\rho_w = 1027\ \mathrm{kg\,m^{-3}}$ throughout; all other parameters are varied.

Under the hydrostatic approximation, the vertical normal stress in the glacier is given by

$$\sigma_{zz}(x,z) = -\rho_i g[h(x) - z]. \tag{1}$$

Splitting the stress into deviatoric and pressure parts ($\sigma_{zz} = \tau_{zz} - p$ and $\sigma_{xx} = \tau_{xx} - p$), and taking ice to be incompressible ($\tau_{xx} + \tau_{zz} = 0$), the horizontal normal stress is then (see, e.g., Greve and Blatter, 2009)

$$\sigma_{xx}(x,z) = \tau_{xx} - p = \tau_{xx} - \tau_{zz} + \sigma_{zz} = 2\tau_{xx} - \rho_i g[h(x) - z]. \tag{2}$$

We are aiming to further the implementation of calving laws in the depth-integrated models that are used for large-scale simulation of glaciers and ice sheets. Such models solve only for the depth-integrated or depth-mean value of τ_{xx}, hence we assume that τ_{xx} does not vary with z but return to this point in the discussion.

2.2 Classic crevasse-depth calving law

Within the classic crevasse-depth calving law, dry surface crevasses are assumed to penetrate to a depth where the horizontal normal stress σ_{xx} vanishes (Nye, 1955). Introducing the resistive stress $R_{xx} = 2\tau_{xx}$, which is independent of depth, and using Eq. 2, the fractional surface crevasse depth is

$$\frac{d_s}{H} = \frac{R_{xx}}{\rho_i g H}. \tag{3}$$

Basal crevasses are assumed to penetrate to a height above the bed where the horizontal normal stress plus the crevasse water pressure vanishes:

$$R_{xx} - \rho_i g(H - d_b) + \rho_w g w - \rho_c g d_b = 0. \tag{4}$$

https://doi.org/10.5194/egusphere-2024-2927
Preprint. Discussion started: 17 October 2024

In the classic case of a basal crevasse filled by seawater, where $\rho_c = \rho_w$, Eq. 4 gives the basal crevasse heights of Weertman (1973). Here, we will follow the line of argument of Buck (2023) that the calving process may be impacted by the presence of fresher water in the basal crevasse, hence we retain ρ_c as an independent parameter that may differ from ρ_w. Solving Eq. 4 gives

$$\frac{d_b}{H} = \frac{\rho_i}{\rho_c - \rho_i}\left(\frac{R_{xx}}{\rho_i g H} - \frac{H_{ab}}{H}\right) \tag{5}$$

unless $R_{xx}/\rho_i g H < H_{ab}/H$, in which case there are no basal crevasses. The height above buoyancy, H_{ab}, is given by

$$H_{ab} = \begin{cases} 0 & \text{when } H \leq \frac{\rho_w}{\rho_i} w \text{ (ice is floating)}, \\ H - \frac{\rho_w}{\rho_i} w & \text{when } H > \frac{\rho_w}{\rho_i} w \text{ (ice is grounded below sea level)}. \end{cases} \tag{6}$$

The total crevassed fraction, $f = (d_s + d_b)/H$, is the sum of Eqs. 3 & 5 and is given by

$$f = \begin{cases} \frac{R_{xx}}{\rho_i g H} & \text{when } \frac{R_{xx}}{\rho_i g H} \leq \frac{H_{ab}}{H}, \\ \frac{\rho_c}{\rho_c - \rho_i}\frac{R_{xx}}{\rho_i g H} - \frac{\rho_i}{\rho_c - \rho_i}\frac{H_{ab}}{H} & \text{when } \frac{H_{ab}}{H} < \frac{R_{xx}}{\rho_i g H} < 1 + \frac{\rho_i}{\rho_c}\left(\frac{H_{ab}}{H} - 1\right), \\ 1 & \text{when } \frac{R_{xx}}{\rho_i g H} \geq 1 + \frac{\rho_i}{\rho_c}\left(\frac{H_{ab}}{H} - 1\right), \end{cases} \tag{7}$$

where the first case corresponds to surface crevasses but no basal crevasses, the second case to surface and basal crevasses, and the third case to full crevasse penetration and calving.

To illustrate what these crevasse sizes look like close to the calving front, note that the resistive stress at the calving front can be obtained without an ice sheet model using the boundary condition $\sigma_{xx}(x_{cf}, z) = 0$ above the water and $\sigma_{xx}(x_{cf}, z) = \rho_w g z$ below the water. The resistive stress at the calving front is then

$$R_{xx}(x_{cf}) = \frac{1}{2}\rho_i g H \begin{cases} 1 - \frac{\rho_i}{\rho_w} & \text{when } H \leq \frac{\rho_w}{\rho_i} w \text{ (ice is floating)} \\ 1 - \frac{\rho_w}{\rho_i}\frac{w^2}{H^2} & \text{when } H > \frac{\rho_w}{\rho_i} w \text{ (ice is grounded)} \end{cases} \tag{8}$$

where w and H take their values at the calving front. By using Eq. 8 in Eqs. 3, 5 & 7 we can therefore estimate the crevasse sizes close to the calving front without the use of an ice sheet model.

The resulting crevasse sizes are shown in Fig. 2 as a function of fractional calving front water depth w/H, for the two end-member cases where the basal crevasse is filled with seawater ($\rho_c = \rho_w$) or with freshwater ($\rho_c = \rho_{fw} = 1000\ \mathrm{kg\,m^{-3}}$). Surface crevassing is independent of basal crevasse water density, and is greatest at a dry calving cliff ($w/H = 0$) when there is no ocean water to support the cliff and the resistive stress is largest. As fractional calving front water depth increases, fractional surface crevasse depth decreases, until for glaciers at flotation ($w/H = \rho_i/\rho_w \approx 0.89$) the fractional surface crevassing is roughly 0.06. At dry or well-grounded calving fronts the calving front water depth is insufficient to give basal crevasses; these arise when fractional calving front water depths exceed roughly 0.66. Above this threshold, basal crevasses grow quickly with fractional water depth until at flotation they reach a fractional height of roughly 0.44, assuming the crevasse is filled with seawater, or roughly 0.58, assuming the crevasse is filled with freshwater.

https://doi.org/10.5194/egusphere-2024-2927
Preprint. Discussion started: 17 October 2024

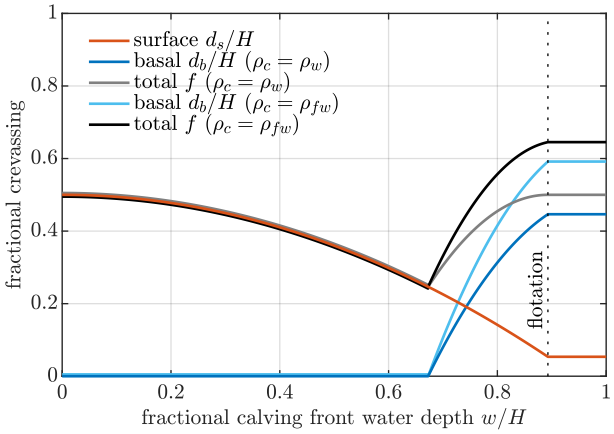

Figure 2. Dependence of crevasse sizes on fractional calving front water depth in the classic crevasse-depth law. This applies only close to the calving front. A fractional calving front water depth of 0 corresponds to a dry calving cliff, a fractional calving front water depth of 0.5 corresponds to a calving front where the ocean depth is half of the ice thickness and a fractional calving front water depth greater than $\rho_i/\rho_w \approx 0.89$ corresponds to a floating calving front. When the basal crevasse is filled with seawater we get the basal crevassing indicated in dark blue and total crevassing indicated in grey. When the basal crevasse is filled with freshwater we get the basal crevassing indicated in light blue and total crevassing indicated in black. Surface crevasse depths are independent of basal crevasse water density. Note that this plot applies regardless of ice thickness.

The key point of Fig. 2 for the present study is that the total fractional crevassing never reaches 1. For the case of seawater-filled basal crevasses, the maximum crevassed fraction is 0.5, occurring at a dry front entirely due to surface crevassing, or at a floating front due mostly to basal crevassing. If basal crevasses are filled with freshwater, then the water pressure in the basal crevasse falls away more slowly with height, giving larger basal crevasses. However, the total fractional crevassing still does not exceed ≈0.66, occurring for glaciers at flotation (Fig. 2).

In its classic form, therefore, the crevasse-depth calving law applied to a calving front predicts that calving should never occur. This has motivated the modifications described in the introduction, which either add more stress to the formulation (in the case of water in surface crevasses, Weertman, 1973; Nick et al., 2010) or relax the requirement for calving to occur only when $f = 1$ (in the case of calving once a surface crevasse reaches the waterline, Benn et al., 2007).

An alternative approach, proposed by Buck (2023) for the case of rifts at floating ice shelves, is to account for the concentration of horizontal stress due to the presence of crevassing, and the feedback of this concentration on crevasse size. We now apply that approach to grounded tidewater glaciers.

2.3 Modified formulation for crevasse sizes

Following Buck (2023), we assume that the presence of crevasses modifies the horizontal normal stress to σ'_{xx}. If hydrostatic balance still applies, the vertical normal stress is unmodified and following Eq. 2, we assume that the modified horizontal

https://doi.org/10.5194/egusphere-2024-2927
Preprint. Discussion started: 17 October 2024

normal stress in the intact ice can be written

$$\sigma'_{xx}(x,z) = R'_{xx}(x) - \rho_i g[h(x) - z], \tag{9}$$

where R'_{xx} is the modified resistive stress in the intact ice. In the crevassed ice, the horizontal normal stress has to balance the fluid pressure in the crevasse, giving in total

$$\sigma'_{xx}(x,z) = \begin{cases} 0 & h \geq z > h - d'_s, \\ R'_{xx}(x) - \rho_i g[h(x) - z] & h - d'_s > z > -w + d'_b, \\ \rho_c g z - (\rho_w - \rho_c) g w & -w + d'_b \geq z > -w, \end{cases} \tag{10}$$

where d'_s and d'_b are the modified surface and basal crevasse sizes. Continuing to follow Buck (2023), we insist that the horizontal force balance is conserved under crevassing, so that

$$\int_{-w(x)}^{h(x)} \sigma_{xx}(x,z)\, dz = \int_{-w(x)}^{h(x)} \sigma'_{xx}(x,z)\, dz, \tag{11}$$

whereas for the classic law, $\sigma_{xx}(x,z) = R_{xx}(x) - \rho_i g[h(x) - z]$ at all depths. Performing the integrals leads to the horizontal force balance

$$(H - d'_s - d'_b)\, R'_{xx} = H R_{xx} - \frac{1}{2}\rho_i g d'^2_s - \frac{1}{2}\rho_i g \left(2H d'_b - d'^2_b\right) + \rho_w g w d'_b - \frac{1}{2}\rho_c g d'^2_b. \tag{12}$$

The modified crevasse sizes themselves are then defined just as for the classic law (Eqs. 3 & 5) but replacing the resistive stress with the modified resistive stress. For reasons that will become apparent later, we also include a tensile strength for ice, σ_{max}, so that the modified crevasse sizes are

$$\frac{d'_s}{H} = \frac{R'_{xx} - \sigma_{max}}{\rho_i g H} \tag{13}$$

unless $R'_{xx} < \sigma_{max}$, in which case there are no surface crevasses, and

$$\frac{d'_b}{H} = \frac{\rho_i}{\rho_c - \rho_i}\left(\frac{R'_{xx} - \sigma_{max}}{\rho_i g H} - \frac{H_{ab}}{H}\right) \tag{14}$$

unless $(R'_{xx} - \sigma_{max})/\rho_i g H < H_{ab}/H$, in which case there are no basal crevasses. Eqs. 12, 13 & 14 are then three equations in the three unknowns R'_{xx}, d'_s and d'_b, which can be solved analytically to give the modified crevasse sizes.

When the ice is grounded (i.e., when $H > \frac{\rho_w}{\rho_i} w$), the solution for surface crevasse depths is

$$\frac{d'_s}{H} = \begin{cases} 0 & \text{[A]}, \\ 1 - \tilde{\sigma}_{max} - \sqrt{1 - 2\tilde{R}_{xx} + \tilde{\sigma}^2_{max}} & \text{[B]}, \\ 1 - \frac{\rho_w}{\rho_c}\frac{w}{H} - \tilde{\sigma}_{max} - \sqrt{\left(1 - \frac{\rho_i}{\rho_c}\right)\left(1 - \frac{\rho_w^2 w^2}{\rho_i \rho_c H^2} - 2\tilde{R}_{xx}\right) + \tilde{\sigma}^2_{max}} & \text{[C]}, \end{cases} \tag{15}$$

https://doi.org/10.5194/egusphere-2024-2927
Preprint. Discussion started: 17 October 2024

and basal crevasse heights

$$\frac{d_b'}{H} = \begin{cases} 0 & \text{[A]}, \\ 0 & \text{[B]}, \\ \frac{\rho_w}{\rho_c}\frac{w}{H} - \frac{\rho_i}{(\rho_c-\rho_i)}\left[\tilde{\sigma}_{max} + \sqrt{\left(1-\frac{\rho_i}{\rho_c}\right)\left(1-\frac{\rho_w^2 w^2}{\rho_i\rho_c H^2} - 2\tilde{R}_{xx}\right) + \tilde{\sigma}_{max}^2}\right] & \text{[C]}, \end{cases} \tag{16}$$

in which for convenience we have defined $\tilde{R}_{xx} = R_{xx}/\rho_i g H$ and $\tilde{\sigma}_{max} = \sigma_{max}/\rho_i g H$. The solutions [A] apply when the surface crevasse depth, as given by solutions [B], is not positive. This gives the condition $\tilde{R}_{xx} \leq \tilde{\sigma}_{max}$ (or equivalently $R_{xx} \leq \sigma_{max}$), which is when the resistive stress is smaller than the tensile strength of the ice and hence there is no surface or basal crevassing. The solutions [B] apply when the solutions [A] do not apply, and when the basal crevasse height, as given by solutions [C], is not positive. This gives the condition

$$\tilde{\sigma}_{max} < \tilde{R}_{xx} \leq \frac{1}{2} + \tilde{\sigma}_{max}\frac{\rho_w w}{\rho_i H} - \frac{1}{2}\left(\frac{\rho_w w}{\rho_i H}\right)^2, \tag{17}$$

which is when the resistive stress is sufficient to give surface crevassing but the water depth is insufficient to give basal crevassing. Finally, the solutions [C] apply when neither [A] nor [B] holds and is when there are both surface and basal crevasses.

For ice at flotation ($\rho_w w = \rho_i H$), the right hand side of the inequality in Eq. 17 reduces to $\tilde{\sigma}_{max}$, meaning that the threshold for the existence of both surface and basal crevasses is $\tilde{R}_{xx} > \tilde{\sigma}_{max}$. For floating ice, therefore, there are either no crevasses at all or there are basal and surface crevasses. The crevasse sizes are therefore either 0 or are given by the [C] expressions after making the substitution $\rho_w w \to \rho_i H$.

Within a depth-integrated ice sheet simulation the model would provide R_{xx}, from which the surface and basal crevasse sizes can be calculated using Eqs. 15 & 16. As before, however, we can proceed without an ice sheet model and see the implications of the modified calving law using the expression for the resistive stress at the calving front. All of the following results are therefore obtained by substituting Eq. 8 into Eqs. 15 & 16.

3 Results

The results section proceeds by first showing an illustrative example of the modified crevasse sizes (section 3.1), then exploring the sensitivity of the predicted crevasse sizes to ice tensile strength, basal crevasse water density and ice thickness (sections 3.2 & 3.3). After building this understanding of the modified crevasse sizes we consider the implications for calving (section 3.4), which motivates the final results section where we consider the role of basal friction (section 3.5).

3.1 An illustrative example

The modified crevasse sizes are a complex function of calving front water depth w, ice thickness H, tensile strength σ_{max} and crevasse water density ρ_c. This contrasts with the classic crevasse-depth law, in which the crevasse sizes are a function of the

https://doi.org/10.5194/egusphere-2024-2927
Preprint. Discussion started: 17 October 2024

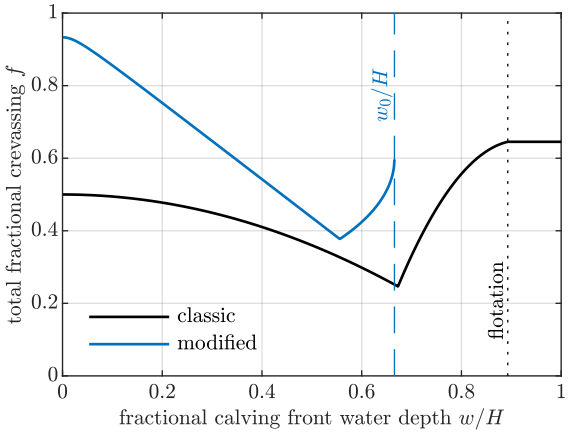

Figure 3. Illustrative example of the modified crevasse sizes, compared to the classic law, showing total fractional crevassing plotted against fractional ocean water depth at the calving front. Here, $\rho_c = 1000\ \mathrm{kg\,m^{-3}}$. The modified crevasse sizes additionally requires that we specify $H = 500$ m and $\sigma_{max} = 150$ kPa. The blue dashed vertical line indicates the fractional water depth w_0/H above which the modified crevasse sizes have no real solution.

ratio w/H only (and possibly the crevasse water density if that is allowed to vary). To begin to explore the modified law, we consider an illustrative example with a fixed calving front ice thickness of $H = 500$ m, representing a relatively large tidewater glacier. We also take $\rho_c = 1000\ \mathrm{kg\,m^{-3}}$ (i.e., the basal crevasse is filled with freshwater) and a tensile strength $\sigma_{max} = 150$ kPa.

The total crevassed fraction $f = (d'_s + d'_b)/H$ (sum of surface and basal crevassing) is shown in Fig. 3. In common with the classic crevasse-depth law, for dry calving cliffs or very well-grounded glaciers, there are no basal crevasses and the crevassed fraction decreases as the water depth increases. However, the modified crevassed fraction is significantly larger than in the classic law. From Eq. 17, basal crevasses are present when

$$\frac{w}{H} > \frac{2\rho_i}{\rho_w - \rho_i}\frac{\sigma_{max}}{\rho_i g H} \tag{18}$$

unless this exceeds flotation, in which case there are no basal crevasses for any water depth. For the particular parameters we have chosen in Fig. 3, basal crevasses are present in the modified law for fractional water depths greater than about 0.57 (observed as the sharp corner in the fractional crevassing). For larger water depths, the crevassed fraction quickly increases as the basal crevasses get larger. Above a critical fractional water depth w_0/H, which takes a value of ≈ 0.65 in Fig. 3, the term in the square root in Eqs. 15 & 16 becomes negative and the crevassed fraction is undefined. We interpret this as calving and explore this in section 3.4.

https://doi.org/10.5194/egusphere-2024-2927
Preprint. Discussion started: 17 October 2024

3.2 Dependence on basal crevasse water density and ice tensile strength

The features observed in the illustrative example depend strongly on the density of water in the basal crevasse and on ice tensile strength. For an ice thickness $H = 500$ m and tensile strength $\sigma_{max} = 150$ kPa, the sensitivity to basal crevasse water density is shown in Fig. 4a. Crevasse water density does not affect the result when only surface crevasses are present ($w/H < 0.57$ in Fig. 4a). Once basal crevasses are present, they grow much more quickly with water depth when the crevasse water density is smaller. Or equivalently, for a given water depth, basal crevasses are larger when the crevasse water density is smaller. This effect arises because when the crevasse water density is smaller, the water pressure in the crevasse falls away more slowly with height above the bed, hence the water pressure in the basal crevasse is higher. For the lower values of crevasse water density considered (1000 and 1009 kg m^{-3} in Fig. 4a), there are water depths beyond which no real solution for crevasse size exists. For crevasse water density of 1018 kg m^{-3}, a real solution for crevasse sizes exists for all fractional water depths. When crevasses are filled with seawater of density 1027 kg m^{-3}, and when $w/H > 0.57$, the increase in basal crevasse height with water depth is balanced by the decrease in surface crevasse depth, giving a constant total fractional crevassing. In our framework, therefore, the existence and impact of basal crevasses depends sensitively on the density of water in the basal crevasse.

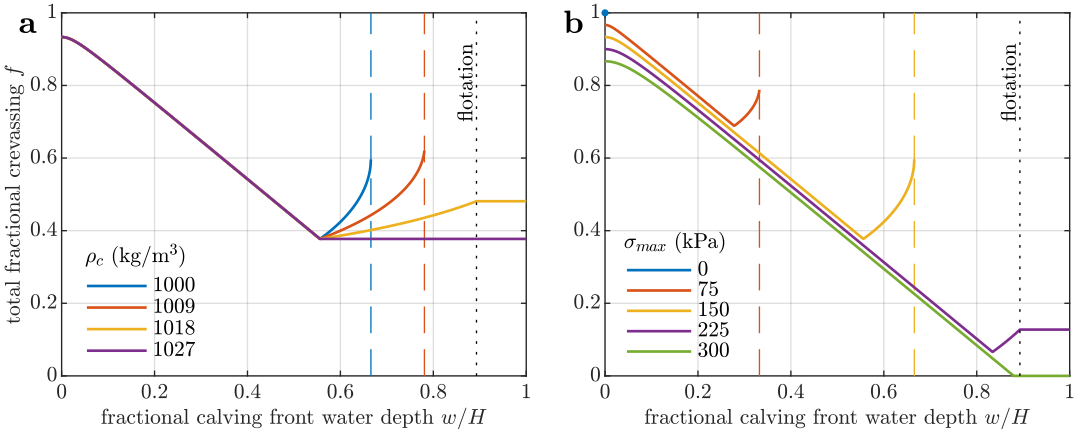

Figure 4. Dependence of total fractional crevassing on (a) crevasse water density, and (b) ice tensile strength. The ice thickness is $H = 500$ m and in (a) the ice tensile strength is $\sigma_{max} = 150$ kPa while in (b) the crevasse water density is $\rho_c = 1000$ kg m^{-3}. The vertical dashed lines indicate w_0/H - the fractional water depth above which the modified crevasse sizes have no real solution. In (b), note that the only real solution for $\sigma_{max} = 0$ kPa is $f = 1$ at $w/H = 0$.

Crevassing also depends strongly on the assumed ice tensile strength (Fig. 4b). For larger tensile strength, the depth of surface crevasses is smaller and greater water depths are required to generate basal crevasses. Noting that the results in Fig. 4b depend on the assumed values $H = 500$ m and $\rho_c = 1000$ kg m^{-3}, there is no real solution for crevasse sizes beyond a fractional water depth of 0.33 when $\sigma_{max} = 75$ kPa or 0.65 when $\sigma_{max} = 150$ kPa. For $\sigma_{max} = 225$ kPa there are basal crevasses for

https://doi.org/10.5194/egusphere-2024-2927
Preprint. Discussion started: 17 October 2024

large water depths and there is a real solution for all water depths, while for $\sigma_{max} = 300$ kPa there are no basal crevasses for any water depth.

When ice is assumed to have zero tensile strength ($\sigma_{max} = 0$ kPa), as in the classic crevasse-depth calving law, our framework either gives no real crevasse size solutions (when $\rho_c < 1027\ \mathrm{kg\,m^{-3}}$ and $w/H > 0$) or always gives a crevassed fraction of 1 (when $\rho_c = 1027\ \mathrm{kg\,m^{-3}}$). For zero tensile strength, the modified crevasse-depth law therefore predicts that no calving front could ever exist; this is why we introduced the non-zero tensile strength into Eqs. 13 & 14.

3.3 Dependence on ice thickness

We can also fix the basal crevasse water density and ice tensile strength and consider the sensitivity of crevassing to ice thickness (Fig. 5). For sufficiently small ice thickness ($H = 100$ or 300 m in Fig. 5, where $\sigma_{max} = 150$ kPa and $\rho_c = 1000\ \mathrm{kg\,m^{-3}}$), there are no basal crevasses present for any water depth. As ice thickness increases beyond this, basal crevasses form at smaller fractional water depths and for sufficiently large water depth no real solution exists for the crevasse sizes. For $H = 900$ m, there is no real solution for crevasse sizes beyond a fractional water depth of ≈ 0.37. The dependence of crevasse size on ice thickness in the modified crevasse-depth law contrasts with the classic crevasse-depth law, in which there is no dependence on ice thickness. The difference arises from the introduction of a non-zero ice tensile strength in the modified law.

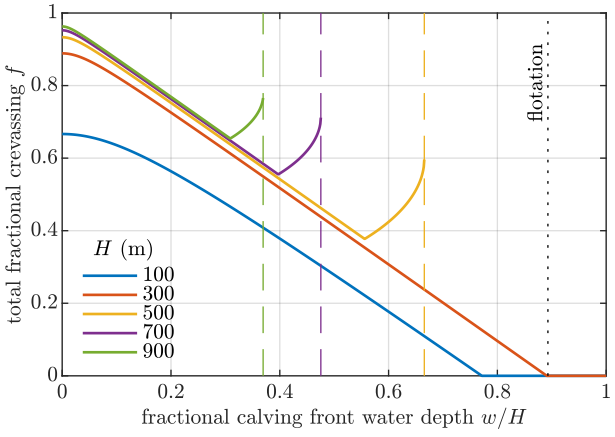

Figure 5. Dependence of total fractional crevassing on ice thickness. The ice tensile strength is $\sigma_{max} = 150$ kPa and the basal crevasse water density is $\rho_c = 1000\ \mathrm{kg\,m^{-3}}$. The vertical dashed lines again indicate w_0/H.

3.4 Modified conditions for calving

Calving can occur when the total fractional crevassing reaches 1, but in this modified crevasse-depth law that only occurs in the case of zero ice tensile strength. And, when we do assume zero tensile strength, the total fractional crevassing is either 1 or undefined for all possible calving fronts (e.g., Fig. 4b), hence this is not a useful calving law.

https://doi.org/10.5194/egusphere-2024-2927
Preprint. Discussion started: 17 October 2024

The other possibility for calving, seen throughout Figs. 3–5, occurs when the term in the square root in Eqs. 15 & 16 becomes negative and there is no longer a real solution for the crevasse sizes. This means that it is no longer possible, with physical crevasse sizes, to satisfy the horizontal force balance (Eq. 12) and we interpret this as triggering calving. This possibility does not arise in the classic crevasse-depth calving law. The water depth at which this occurs is

$$w_0 = \left[\frac{\rho_i \rho_c^2}{\rho_w(\rho_c - \rho_i)(\rho_w - \rho_c)}\right]^{1/2} \frac{\sigma_{max}}{\rho_i g}. \tag{19}$$

The implication of the modified calving criterion is that, for grounded glaciers, calving occurs when the absolute water depth exceeds w_0. If the ice reaches flotation before it reaches w_0, then calving never occurs by this criterion. For ice to reach flotation before reaching w_0, the ice thickness must be less than

$$H_0 = \frac{\rho_w}{\rho_i} w_0 = \tilde{\rho} \frac{\sigma_{max}}{\rho_i g}, \tag{20}$$

where

$$\tilde{\rho} = \left[\frac{\rho_w \rho_c^2}{\rho_i(\rho_c - \rho_i)(\rho_w - \rho_c)}\right]^{1/2} \tag{21}$$

The modified calving criterion is therefore an upper bound on the frontal water depth at grounded glaciers and an upper bound on the frontal ice thickness at ice shelves.

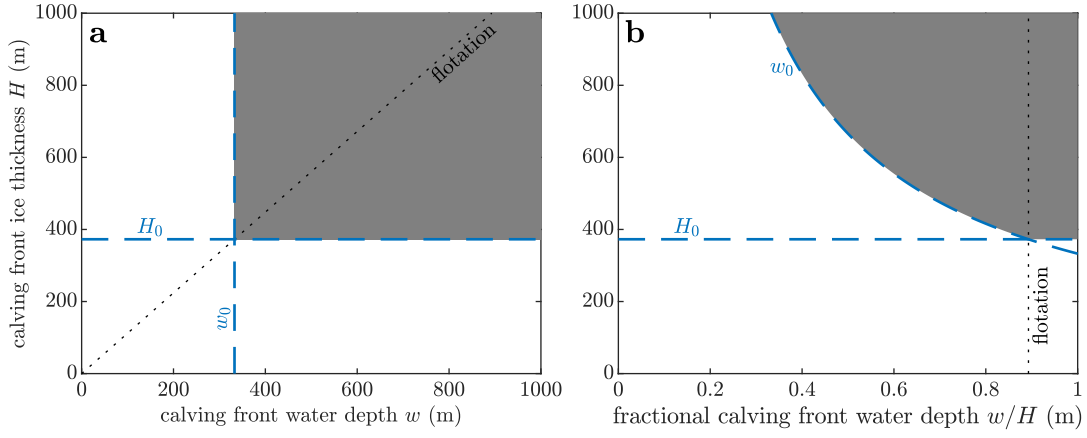

Figure 6. Illustration of the modified calving criterion described in section 3.4; shaded regions are combinations of ice thickness and water depth that would calve according to the calving criterion of Eqs. 19 & 20. The sub-panels are equivalent but (a) has absolute calving front water depth on the x-axis while (b) has fractional calving front water depth on the x-axis. Grounded calving fronts lie to the left of the black dotted lines; floating calving fronts are to the right. The adjustable parameters are $\rho_c = 1000\ \mathrm{kg\,m^{-3}}$ and $\sigma_{max} = 150$ kPa.

The calving criterion can be visualised in plots of calving front ice thickness versus calving front water depth (Fig. 6a) or fractional calving front water depth (Fig. 6b). In such plots, the calving criterion separates stable and unstable combinations of

https://doi.org/10.5194/egusphere-2024-2927
Preprint. Discussion started: 17 October 2024

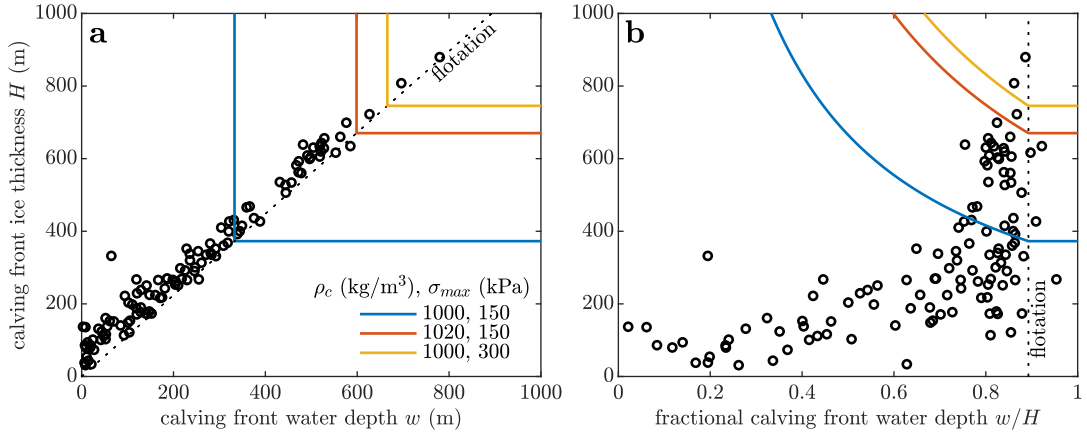

Figure 7. Version of Fig. 6 showing the sensitivity of the calving criterion to water density in the basal crevasse and to ice tensile strength. For the given parameter values, frontal ice thickness and water depth combinations that lie up and right of the coloured lines are unstable to calving (as was indicated by shading in Fig. 6). The black markers show observed calving front ice thickness and water depth values from Ma et al. (2017).

frontal ice thickness and water depth. Unstable combinations are either glaciers grounded in water depths that exceed w_0, or floating glaciers with a frontal ice thickness that exceeds H_0.

The separation into stable and unstable regions clearly depends on the assumed basal crevasse water density and the tensile strength of ice (Fig. 7; see also Fig. 4). Higher basal crevasse water density and ice tensile strength makes more of the parameter space stable and increases the water depth and ice thickness required for calving. Fig. 7 also includes real-world ice thickness and water depth combinations from Ma et al. (2017). These observations were derived from IceBridge radar profiles (CReSIS, 2024) at 30 glaciers in Greenland, some at multiple points in time during 2006-2014. As noted in Ma et al. (2017), and similarly in Bassis and Walker (2012), these observations tend to cluster near the line of flotation, particularly for large ice thicknesses (Fig. 7). The presence of glaciers existing stably for a number of years in a region of the plot that our calving criterion would say is unstable invalidates certain choices of the basal crevasse water density and ice tensile strength. For example, with $\rho_c = 1000$ kg m^{-3} and $\sigma_{max} = 150$ kPa, our calving criterion suggests that any grounded glaciers with a water depth exceeding 330 m should not stably exist, which is clearly contradicted by the observations (Fig. 7a). Making the ice stronger ($\sigma_{max} = 300$ kPa) results in most of the observations lying within the stable regime as defined by the calving criterion. However, the calving criterion still does not look very promising as a calving law, in the sense that it does not explain much about the distribution of observed calving front ice thickness and water depth combinations. This motivates a further modification to the crevasse-depth formulation, outlined in the next section.

https://doi.org/10.5194/egusphere-2024-2927
Preprint. Discussion started: 17 October 2024

3.5 Possible role of basal friction

Suppose that the surface–basal crevasse pair that may result in calving is located a distance L from the calving front (Fig. 1) and that the basal shear stress resulting from ice–bed contact over that distance is τ_b. The distance L could represent a typical crevasse spacing and, since tidewater glaciers are generally densely crevassed close to their fronts, is imagined to be on the order of H or smaller. Neglecting other factors that change the stress along-flow, such as bed or ice surface slope, the resistive stress at the crevasse pair can be estimated as

$$R_{xx}(x_{cf} - L) \approx \frac{1}{2}\rho_i g H \left(1 - \frac{\rho_w}{\rho_i}\frac{w^2}{H^2}\right) - \frac{L}{H}\tau_b \tag{22}$$

which applies only for grounded glaciers because otherwise there is no ice–bed contact. If we use Eq. 22 in the modified crevasse sizes Eqs. 15 & 16 (instead of the previously-used Eq. 8) then for grounded glaciers, calving occurs when the water depth exceeds

$$w_1 = w_0\sqrt{1 + 2\left(1 - \frac{\rho_i}{\rho_c}\right)\frac{\tilde{\tau}_b\tilde{L}}{\tilde{\sigma}^2_{max}}} \tag{23}$$

where $\tilde{\tau}_b = \tau_b/\rho_i g H$, $\tilde{L} = L/H$ and w_0 is given by Eq. 19. It is also useful to have the ice thickness when Eq. 23 is at flotation, which can be written as

$$H_1 = H_0\sqrt{1 + 2\left(1 - \frac{\rho_i}{\rho_c}\right)\frac{\tilde{\tau}_b\tilde{L}}{\tilde{\sigma}^2_{max}}} \tag{24}$$

where H_0 is given by Eq. 20.

The effect of basal friction on the calving criterion is illustrated in Fig. 8. Basal friction reduces the resistive stress driving calving and therefore increases the water depth required to trigger calving from w_0 (Eq. 19) to w_1 (Eq. 23). Of course, Eq. 23 applies only for grounded glaciers and so the parameter space effectively splits into 3 regions (Fig. 8). These are (i) $H < H_0$, where both w_0 and w_1 are larger than the flotation water depth and so no calving occurs by our criterion; (ii) $H_0 < H < H_1$, where basal friction allows water depths larger than w_0 to be stable, but the basal friction is lost at flotation and so the glaciers calve at flotation; (iii) $H > H_1$, where we reach w_1 before flotation and so glaciers calve at water depth w_1. Comparing Fig. 8 and Fig. 6 shows that by our criterion, basal friction stabilises grounded glaciers with a frontal ice thickness between H_0 and H_1 (or equivalently with a frontal water depth between w_0 and w_1).

The calving front ice thicknesses H_0 and H_1 depend on a number of parameters (Fig. 9). H_0, in this framework, principally depends on the basal crevasse water density and the ice tensile strength (see also Fig. 7), so that varying the ice tensile strength changes the ice thicknesses that produce calving at flotation (Fig. 9, blue vs red). H_1 also depends on the basal crevasse water density and the ice tensile strength, but additionally on the basal shear stress and the crevasse spacing. Increasing either of the latter two quantities increases H_1, and so more of the grounded parameter space is stable to calving (Fig. 9, yellow and purple).

Considering the distribution of observed calving front ice thickness and water depth combinations, the introduction of basal friction provides a better explanation for some of the distribution, because it provides a reason why many of the glaciers have

https://doi.org/10.5194/egusphere-2024-2927
Preprint. Discussion started: 17 October 2024

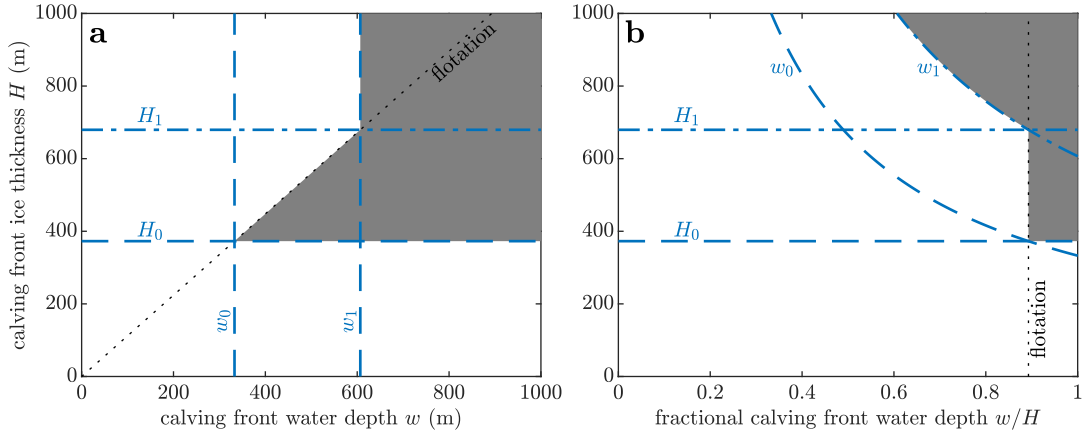

Figure 8. Illustration of the impact of basal friction on the calving criterion. w_0 and H_0 define the calving regime when there is no basal friction (as in Fig. 6). Basal friction introduces a new water depth, w_1, and the ice thickness at which w_1 crosses flotation is denoted H_1. The calving front ice thickness and water depth combinations that are unstable to calving are shaded grey. The adjustable parameters take values $\rho_c = 1000\ \mathrm{kg\,m^{-3}}$, $\sigma_{max} = 150$ kPa, $\tau_b = 70$ kPa and $L = 500$ m.

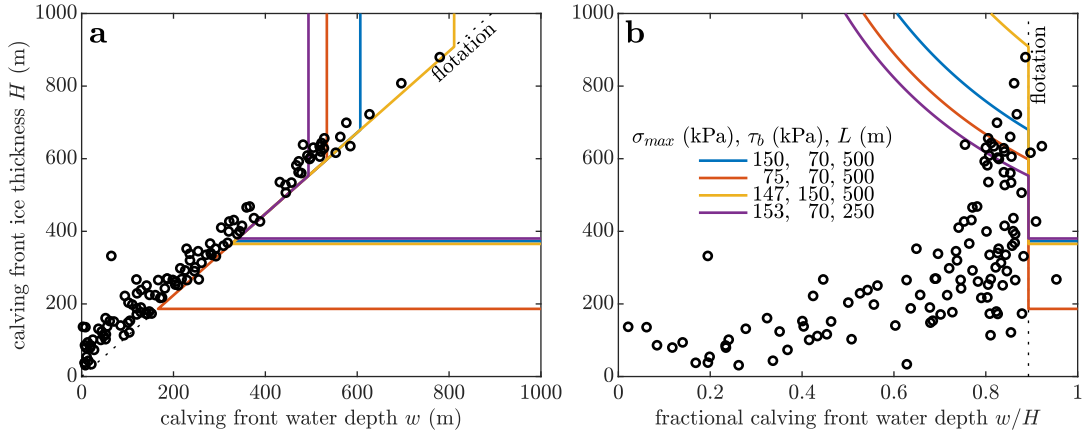

Figure 9. Version of Fig. 8 showing the sensitivity of the calving criterion to adjustable parameters (though all results shown assume $\rho_c = 1000\ \mathrm{kg\,m^{-3}}$). For the given parameter values, frontal ice thickness and water depth combinations that lie to the right of the coloured lines are unstable to calving (as indicated by shading in Fig. 8). The black markers show observed calving front ice thickness and water depth values from Ma et al. (2017).

flotation as a lower bound on their frontal ice thickness, or upper bound on their frontal water depth. However, relatively large values of basal friction, exceeding 150 kPa, are required to make the largest glaciers stable to calving by our criterion (though this value depends also on the assumed basal crevasse water density, ice tensile strength and crevasse spacing).

https://doi.org/10.5194/egusphere-2024-2927
Preprint. Discussion started: 17 October 2024

4 Discussion

4.1 A modified crevasse-depth calving criterion

Motivated by the fact that the crevasse-depth approach is a natural and promising formulation for calving, but that in its classic form it predicts no calving, we have applied the approach of Buck (2023) to crevasses at grounded tidewater glaciers. This approach results in two modifications to the classic crevasse-depth law. First, it provides a simple means of accounting for the impact of crevasses on the stress field, and thereafter for the feedback of the crevasse-modified stress on the crevasse sizes. Since the resistive stress concentrates under crevassing, the obtained crevasses are deeper than in the classic law (Fig. 3). Second, it allows for fresher water in basal crevasses, which leads to higher water pressure in the basal crevasse and larger crevasses (Figs. 2 & 4a). To these modifications we have further added a non-zero tensile strength and accounted for basal friction.

Having all of these modifications is central to the outcome. Modifying only the density of water in basal crevasses does not give significantly larger crevasses (Fig. 2). Accounting only for the stress concentration, while having seawater in the basal crevasses gives either (i) full-depth crevassing in every situation when ice has zero tensile strength, or (ii) never full-depth crevassing when ice has non-zero tensile strength. Accounting for the stress concentration and varying the density of water in basal crevasses gives the happy medium required for a calving law: that is, some calving front geometries are stable and some are unstable. The final addition of basal friction is motivated by observations (e.g., Fig. 9) and leads to the behaviour of calving at flotation for some frontal ice thicknesses.

Mathematically, calving in the modified law appears in an unexpected way. Rather than the surface and basal crevasses stably and gradually fracturing the full thickness, as would happen in the classic law with water in the surface crevasses, it becomes impossible to satisfy the horizontal force balance for the nascent calving block so that the crevasse sizes become undefined. Physically, this might represent the situation where a grounded calving front is advancing into deeper water and the fractional crevassing is slowly increasing, until at a certain water depth the forces on the nascent calving block cannot be balanced, so the block accelerates relative to the glacier and the fracturing of the remaining ice thickness occurs very quickly.

Although the algebra is involved and there are a significant number of parameters in this modified formulation, the final modified calving criterion is actually rather simple (illustrated in the cartoon of Fig. 10). The modified formulation suggests that calving front ice thicknesses less than $H_0 = \tilde{\rho}\sigma_{max}/\rho_i g$ (Eq. 20) do not reach sufficiently high horizontal stresses to calve by this mechanism. If we introduce basal friction, then calving fronts with ice thickness between H_0 and H_1 (the latter given by Eq. 24) will calve at flotation, because basal friction is the factor stopping them from calving. For calving front ice thicknesses greater than H_1, the modified formulation predicts that calving should occur when they are grounded and reach a water depth of w_1 (Eq. 23). However, this last calving regime is possibly the least physically-relevant, because Bassis and Walker (2012) have shown that well-grounded glaciers with large ice thicknesses are likely unstable to shear failure. This shear failure might prohibit any glaciers from obtaining the required geometry to fail at the water depth w_1.

https://doi.org/10.5194/egusphere-2024-2927
Preprint. Discussion started: 17 October 2024

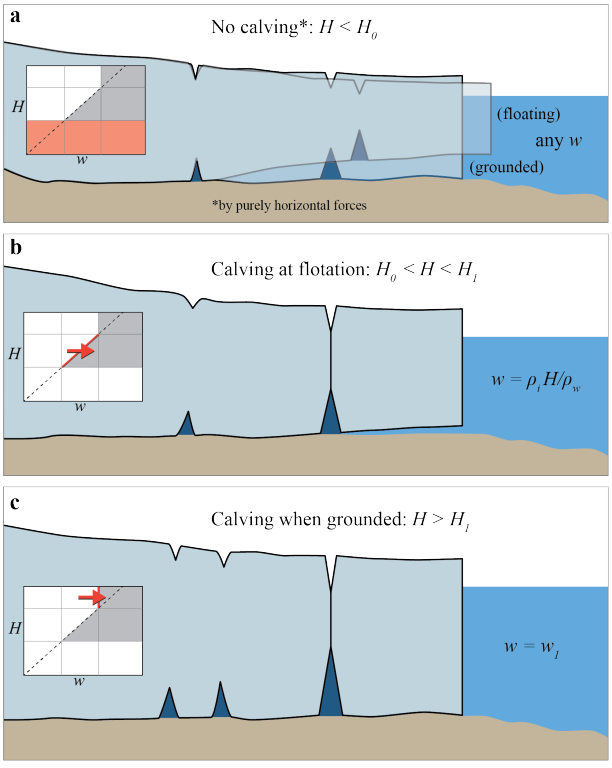

Figure 10. Cartoon of three thickness regimes, illustrating the modified crevasse-depth calving criterion proposed here. Insets on the left show schematics of Fig. 8, illustrating (a) the thickness regime for which no calving occurs (red rectangle) and (b,c) the transitions from stable to unstable water depths for floating and grounded glaciers respectively (red arrows).

4.2 Interpretation in terms of calving styles

By the methodology that we have chosen, the calving style in this study is full-thickness and driven purely by horizontal forces. Our results suggest that this calving style occurs at flotation for calving front ice thicknesses between H_0 and H_1, but that it does not occur for calving front ice thicknesses less than H_0, so that H_0 appears as a thickness threshold above which this calving style appears (Figs. 8 & 9). If the basal crevasses are assumed to be filled with freshwater, and we take a value $\sigma_{max} = 150$ kPa for the effective tensile strength of ice (following results by Grinsted et al. (2024)) then Eq. 20 gives $H_0 \approx 400$ m.

Goliber and Catania (2024) recently inferred the calving style of 10 glaciers in Greenland over recent decades, categorising into low-frequency, full-thickness events that they termed ‘buoyant flexure’, and high-frequency low-volume events that they termed ‘serac failure’. We suggest that their buoyant flexure style, being full thickness and occurring close to flotation, is closely related to the full thickness calving that occurs in our framework for ice thicknesses between H_0 and H_1. In Goliber and Catania (2024), the three glaciers with the greatest frontal ice thickness (600–800 m) were assigned a dominant style of

https://doi.org/10.5194/egusphere-2024-2927
Preprint. Discussion started: 17 October 2024

buoyant flexure. Three glaciers with small frontal ice thickness (100-300 m) were assigned a dominant style of serac failure. The remaining four glaciers had a mixed style, or a style that varied through time, and had intermediate frontal ice thickness (250–450 m). In particular, they showed that Sermeq Silardleq calved mostly by serac failure when its frontal ice thickness was approximately 300 m and, after retreating, calved mostly by buoyant flexure when its frontal ice thickness was approximately 450 m. From this and other studies (e.g., Fried et al., 2018), there is therefore good observational evidence that calving style is influenced by ice thickness and that full-thickness calving occurs predominantly for thicker ice. Additionally, the thickness threshold above which full-thickness calving occurs in our theory, $H_0 \approx 400$ m, appears in good agreement between our theory and the observations.

The thickness threshold H_0 is essentially the maximum ice thickness that unconfined, crevassed ice can support without horizontal stresses pulling it apart (for a given ice tensile strength and ice and water density values). At unconfined floating ice shelves, it should then provide an upper bound on the calving front thickness. Observational evidence supporting both the interpretation and the value of H_0 can therefore be found at, for example, the calving front of the Ross Ice Shelf, which has a maximum thickness approaching 400 m (Becker et al., 2021, their Fig. 2d).

For frontal ice thicknesses exceeding H_0, but not larger than H_1, our results suggest that calving should occur at flotation. As noted in Bassis and Walker (2012) and Ma et al. (2017) – the latter provides the observations plotted on Figs. 7 & 9 – flotation does provide a good bound on the observed calving front ice thickness and water depth combinations of large Greenland tidewater glaciers. Bassis and Walker (2012), knowing that the classic crevasse-depth law did not give large enough crevasses to drive calving at flotation, provided a heuristic argument that this bound could be obtained analytically by assuming calving when ice at the base of the front reached a yield stress. Ma et al. (2017) considered an evolving glacier in a full-Stokes framework and found that glaciers with a free-slip basal boundary condition thinned to nearly flotation, at which point surface and basal crevasses intersected and calving occurred.

Our study provides a different route to the flotation bound that appears in observations. The bound in our study uses the analytical crevasse-depth framework, modified to account for the feedback between crevassing and the stress field, and arises because certain frontal ice thicknesses are stable in the presence of basal friction but unstable without. Therefore, when such a calving front reaches flotation it loses its basal friction, becomes unstable and calves. There is an important difference in our bound, relative to those before, however, which is that our bound applies only for ice thicknesses exceeding H_0. This thickness scale is not present in previous crevasse-depth studies and arises here due to the inclusion of a non-zero ice tensile strength (a similar scale does exist in linear elastic fracture mechanics approaches provided there is a non-zero fracture toughness).

Our results predict no calving at all for glaciers with frontal ice thicknesses less than H_0 (Fig. 8), meaning that this formulation is incomplete as a calving law for Greenland's glaciers in general. But perhaps that is as it should be – this study has considered only horizontal forces, and so we could infer that calving at glaciers with smaller calving front ice thickness is not driven purely by horizontal forces. This is in agreement with studies of calving at smaller glaciers that suggest an important role for melt undercutting and serac failure (e.g., Luckman et al., 2015; Fried et al., 2018; How et al., 2019; Wagner et al., 2019; Goliber and Catania, 2024); processes in which rotational and vertical forces likely play an important role (Slater et al.,

https://doi.org/10.5194/egusphere-2024-2927
Preprint. Discussion started: 17 October 2024

2021). A more general formulation for calving will need to consider these processes too, and will therefore need to go beyond parameterisations or laws that consider only horizontal forces.

4.3 Role of basal friction

The possible inclusion of basal friction within the calving law itself, as opposed to simply as a boundary condition on ice flow, is a subtle issue. There are two ways that our results could be used within an ice sheet model. An ice sheet model could apply Eqs. 15 & 16, substituting in the value of R_{xx} that is calculated by the model, and look for regions where the total fractional crevassing exceeds 1. Or, following our analysis that uses the boundary value of R_{xx} (Eq. 8 or 22), an ice sheet model could instead apply the final calving criterion (Fig. 10) as a condition on the frontal ice thickness. In the former, basal friction enters the stress balance that the model uses to estimate R_{xx}, but it does not enter the calving criterion. In the latter, basal friction enters the calving criterion, which also introduces a typical crevasse spacing L. This notion of a discrete crevasse spacing would not be present in the first approach to implementing our results in an ice sheet model. Since we have argued that the presence of crevasses results in stress concentrations that in turn increase the size of crevasses, it is natural that calving is most likely to occur at crevasses that are advected into the near-terminus region from upstream. From this perspective, it is natural that crevasse spacing would appear in the calving criterion, from which it follows that basal friction on the nascent calving block should be accounted for.

4.4 Limitations

Having discussed where we feel this revised crevasse-depth law matches observations and has important implications, it seems befitting to also consider its weaknesses and the assumptions that were necessary to reach the results.

Firstly, the treatment of stress is highly idealised. This includes the flowline nature of the analysis, and the assumptions of hydrostasy and depth-invariant deviatoric stress close to the calving front and in the presence of crevassing. We feel that these assumptions are justified within the context of an analytical study, and because many of the models that need a better treatment of calving are depth-integrated and so do not resolve variability with depth. Full-Stokes models suggest that these variations in stress close to the front can play a role in calving, and the question remains whether we inescapably need these complex models or whether revised analytical approaches, like that presented here, can be sufficient.

Second, our treatment of the materials involved is simplified, as we have adopted uniform densities of ice and water, uniform ice tensile strength and uniform basal friction, all quantities that may vary in reality. Our results are also quite sensitive to these parameters, as was shown in Figs. 7 & 9. The density of the water filling the basal crevasse is a particular unknown – for a well-grounded glacier it seems reasonable that basal crevasses would be filled with freshwater, but for glaciers closer to flotation it is increasingly recognised that seawater may reach inland of the grounding line (Wilson et al., 2020; Kim et al., 2024). What helps, however, is that despite all of the parameters involved in the analysis, the implications for calving essentially depend only on two thicknesses, H_0 and H_1. If confident in the analysis that leads to them, one could potentially tune those thicknesses directly rather than the underlying physical parameters.

https://doi.org/10.5194/egusphere-2024-2927
Preprint. Discussion started: 17 October 2024

Lastly, we have assumed a simple flowline geometry. Real glaciers are three-dimensional and subject to lateral friction that may reduce stresses relative to the "unconfined" case studied here, therefore making more of the parameter space (e.g., Fig. 9) stable to calving. Similarly, real glaciers may have non-vertical calving fronts. This does not directly affect the horizontal force balance that is central to this study (i.e., Eq. 8 still holds for a non-vertical calving front), but submarine melt-induced undercutting of the calving front does remove a region of ice-bed contact and will therefore affect the ice thickness thresholds that we have suggested characterise calving.

5 Conclusion

The crevasse-depth calving law is a promising candidate for parameterising calving at marine-terminating glaciers, but struggles to predict sufficiently deep crevasses to trigger calving. Inspired by Buck (2023), we modified the crevasse depth law with a simple method to account for the stress concentration under crevassing, a variable density of water in basal crevasses, and non-zero ice tensile strength. We provide revised estimates for surface and basal crevasse size (Eqs. 15 & 16) and show that the revised estimates can give full-thickness crevassing without appealing to water in surface crevasses.

After additionally considering basal friction, the revised crevasse-depth criterion suggests that calving driven purely by horizontal forces (for that is what the crevasse-depth law accounts for) splits into three regimes depending on the ice thickness (Fig. 10). For calving front ice thickness less than a threshold value H_0 (Eq. 20), the horizontal forces are alone not large enough to drive calving. For calving front ice thickness greater than H_0 but less than a second threshold H_1 (Eq. 24), calving occurs when the ice reaches flotation, while for calving front ice thickness exceeding H_1, calving occurs at a critical water depth. Our best estimates for the physical parameters involved give an value for H_0 of roughly 400 m. Thus, the revised crevasse-depth law provides an explanation for observations showing that glaciers with frontal ice thickness exceeding 400 m have a dominant calving style of infrequent full-depth events, while glaciers with smaller thicknesses calve more frequent, serac-type icebergs.

We propose that this revision of the crevasse-depth criterion is a step closer to a better understanding of the calving process, but it is incomplete as a calving law because it provides no reason for glaciers with frontal ice thickness less than 400 m to calve. Rather than seeing this as a limitation, we feel this is appropriate because submarine melting likely plays an important role in calving at such glaciers, and melt undercutting induces significant rotational and vertical imbalances. A more unified treatment of calving will need to treat consistently the horizontal forces that are encapsulated by the crevasse-depth law with the rotational and vertical imbalances that it currently ignores.

Code and data availability. As a largely theoretical paper, this paper used no substantial code. The only data used are the ice thickness/frontal water depth data for Greenland marine-terminating glaciers, available as a supplement to Ma et al. (2017).

https://doi.org/10.5194/egusphere-2024-2927
Preprint. Discussion started: 17 October 2024

Author contributions. DAS conceived the study and the analysis. DAS and TJWW undertook the analysis and wrote the paper.

Competing interests. No competing interests are present.

Acknowledgements. DAS acknowledges support from NERC Independent Research Fellowship NE/T011920/1. TJWW was supported by the NSF Office of Polar Programs through grants # 2148544 and # 2338057.

https://doi.org/10.5194/egusphere-2024-2927
Preprint. Discussion started: 17 October 2024

References

Albrecht, T. and Levermann, A.: Fracture-induced softening for large-scale ice dynamics, The Cryosphere, 8, 587–605, 2014.

Alley, R., Cuffey, K., Bassis, J., Alley, K., Wang, S., Parizek, B., Anandakrishnan, S., Christianson, K., and DeConto, R.: Iceberg calving: regimes and transitions, Annual Review of Earth and Planetary Sciences, 51, 189–215, 2023.

Amaral, T., Bartholomaus, T. C., and Enderlin, E. M.: Evaluation of iceberg calving models against observations from Greenland outlet glaciers, Journal of Geophysical Research: Earth Surface, 125, e2019JF005 444, 2020.

Åström, J. A., Vallot, D., Schäfer, M., Welty, E. Z., O'Neel, S., Bartholomaus, T. C., Liu, Y., Riikilä, T. I., Zwinger, T., Timonen, J., and Moore, J. C.: Termini of calving glaciers as self-organized critical systems, Nature Geoscience, 7, 874–878, https://doi.org/10.1038/ngeo2290, 2014.

Bassis, J. N. and Jacobs, S.: Diverse calving patterns linked to glacier geometry, Nature Geoscience, 6, 833–836, 2013.

Bassis, J. N. and Walker, C. C.: Upper and lower limits on the stability of calving glaciers from the yield strength envelope of ice, Proceedings of the Royal Society A: Mathematical, Physical and Engineering Sciences, 468, 913–931, https://doi.org/10.1098/rspa.2011.0422, 2012.

Becker, M. K., Howard, S. L., Fricker, H. A., Padman, L., Mosbeux, C., and Siegfried, M. R.: Buoyancy-Driven Flexure at the Front of Ross Ice Shelf, Antarctica, Observed With ICESat-2 Laser Altimetry, Geophysical Research Letters, 48, e2020GL091 207, https://doi.org/10.1029/2020GL091207, 2021.

Benn, D. I., Warren, C. R., and Mottram, R. H.: Calving processes and the dynamics of calving glaciers, Earth-Science Reviews, 82, 143–179, https://doi.org/10.1016/j.earscirev.2007.02.002, 2007.

Benn, D. I., Astrom, J., Zwinger, T., Todd, J., Nick, F. M., Cook, S., Hulton, N. R. J., and Luckman, A.: Melt-under-cutting and buoyancy-driven calving from tidewater glaciers: new insights from discrete element and continuum model simulations, Journal of Glaciology, 63, 691–702, https://doi.org/10.1017/jog.2017.41, 2017.

Buck, W. R.: The role of fresh water in driving ice shelf crevassing, rifting and calving, Earth and Planetary Science Letters, 624, https://doi.org/10.1016/j.epsl.2023.118444, 2023.

Choi, Y., Morlighem, M., Wood, M., and Bondzio, J. H.: Comparison of four calving laws to model Greenland outlet glaciers, The Cryosphere, 12, 3735–3746, https://doi.org/10.5194/tc-12-3735-2018, 2018.

Cook, S., Zwinger, T., Rutt, I., O'Neel, S., and Murray, T.: Testing the effect of water in crevasses on a physically based calving model, Annals of Glaciology, 53, 90–96, https://doi.org/10.3189/2012AoG60A107, 2012.

Cook, S. J., Christoffersen, P., and Todd, J.: A fully-coupled 3D model of a large Greenlandic outlet glacier with evolving subglacial hydrology, frontal plume melting and calving, Journal of Glaciology, 68, 486–502, 2022.

Cowton, T. R., Todd, J. A., and Benn, D. I.: Sensitivity of Tidewater Glaciers to Submarine Melting Governed by Plume Locations, Geophysical Research Letters, 46, 11 219–11 227, https://doi.org/10.1029/2019GL084215, 2019.

CReSIS: Multichannel Coherent Radar Depth Sounder (MCoRDS) Data, Lawrence, Kansas, USA. Digital Media, http://data.cresis.ku.edu/, 2024.

Duddu, R., Bassis, J., and Waisman, H.: A numerical investigation of surface crevasse propagation in glaciers using nonlocal continuum damage mechanics, Geophysical Research Letters, 40, 3064–3068, 2013.

Enderlin, E. M. and Bartholomaus, T. C.: Sharp contrasts in observed and modeled crevasse patterns at Greenland's marine terminating glaciers, The Cryosphere, 14, 4121–4133, https://doi.org/10.5194/tc-14-4121-2020, 2020.

Fox-Kemper, B.: Ocean, cryosphere and sea level change, in: AGU fall meeting abstracts, vol. 2021, pp. U13B–09, 2021.

https://doi.org/10.5194/egusphere-2024-2927
Preprint. Discussion started: 17 October 2024

Fried, M. J., Catania, G. A., Stearns, L. A., Sutherland, D. A., Bartholomaus, T. C., Shroyer, E., and Nash, J.: Reconciling Drivers of Seasonal Terminus Advance and Retreat at 13 Central West Greenland Tidewater Glaciers, Journal of Geophysical Research: Earth Surface, 123, 1590–1607, https://doi.org/10.1029/2018JF004628, 2018.

Gao, Y., Ghosh, G., Jiménez, S., and Duddu, R.: A finite-element-based cohesive zone model of water-filled surface crevasse propagation in floating ice tongues, Computing in Science & Engineering, 2023.

Goelzer, H., Nowicki, S., Payne, A., Larour, E., Seroussi, H., Lipscomb, W. H., Gregory, J., Abe-Ouchi, A., Shepherd, A., Simon, E., et al.: The future sea-level contribution of the Greenland ice sheet: a multi-model ensemble study of ISMIP6, The Cryosphere, 14, 3071–3096, 2020.

Goliber, S. A. and Catania, G. A.: Glacier Terminus Morphology Informs Calving Style, Geophysical Research Letters, 51, e2024GL108 530, https://doi.org/10.1029/2024GL108530, 2024.

Grinsted, A., Rathmann, N. M., Mottram, R., Solgaard, A. M., Mathiesen, J., and Hvidberg, C. S.: Failure strength of glacier ice inferred from Greenland crevasses, The Cryosphere, 18, 1947–1957, https://doi.org/10.5194/tc-18-1947-2024, 2024.

Holmes, F. A., van Dongen, E., Noormets, R., Petlicki, M., and Kirchner, N.: Impact of tides on calving patterns at Kronebreen, Svalbard–insights from three-dimensional ice dynamical modelling, The Cryosphere, 17, 1853–1872, 2023.

How, P., Schild, K. M., Benn, D. I., Noormets, R., Kirchner, N., Luckman, A., Vallot, D., Hulton, N. R. J., and Borstad, C.: Calving controlled by melt-under-cutting: detailed calving styles revealed through time-lapse observations, Annals of Glaciology, 60, 20–31, https://doi.org/10.1017/aog.2018.28, 2019.

James, T. D., Murray, T., Selmes, N., Scharrer, K., and O'Leary, M.: Buoyant flexure and basal crevassing in dynamic mass loss at Helheim Glacier, Nature Geoscience, 7, 593–596, https://doi.org/10.1038/ngeo2204, 2014.

Jezek, K. C.: A modified theory of bottom crevasses used as a means for measuring the buttressing effect of ice shelves on inland ice sheets, Journal of Geophysical Research: Solid Earth, 89, 1925–1931, https://doi.org/10.1029/JB089iB03p01925, 1984.

Kim, J. H., Rignot, E., Holland, D., and Holland, D.: Seawater Intrusion at the Grounding Line of Jakobshavn Isbræ, Greenland, From Terrestrial Radar Interferometry, Geophysical Research Letters, 51, e2023GL106 181, https://doi.org/https://doi.org/10.1029/2023GL106181, 2024.

Lai, C.-Y., Kingslake, J., Wearing, M. G., Chen, P.-H. C., Gentine, P., Li, H., Spergel, J. J., and van Wessem, J. M.: Vulnerability of Antarctica's ice shelves to meltwater-driven fracture, Nature, 584, 574–578, https://doi.org/10.1038/s41586-020-2627-8, 2020.

Levermann, A., Albrecht, T., Winkelmann, R., Martin, M. A., Haseloff, M., and Joughin, I.: Kinematic first-order calving law implies potential for abrupt ice-shelf retreat, The Cryosphere, 6, 273–286, 2012.

Luckman, A., Benn, D. I., Cottier, F., Bevan, S., Nilsen, F., and Inall, M.: Calving rates at tidewater glaciers vary strongly with ocean temperature, Nature Communications, 6, https://doi.org/10.1038/ncomms9566, 2015.

Ma, Y. and Bassis, J. N.: The Effect of Submarine Melting on Calving From Marine Terminating Glaciers, Journal of Geophysical Research: Earth Surface, 124, 334–346, https://doi.org/10.1029/2018JF004820, 2019.

Ma, Y., Tripathy, C. S., and Bassis, J. N.: Bounds on the calving cliff height of marine terminating glaciers, Geophysical Research Letters, 44, 1369–1375, https://doi.org/10.1002/2016GL071560, 2017.

Mercenier, R., Lüthi, M. P., and Vieli, A.: Calving relation for tidewater glaciers based on detailed stress field analysis, The Cryosphere, 12, 721–739, 2018.

Miles, B. W. J., Stokes, C. R., and Jamieson, S. S. R.: Simultaneous disintegration of outlet glaciers in Porpoise Bay (Wilkes Land), East Antarctica, driven by sea ice break-up, The Cryosphere, 11, 427–442, https://doi.org/10.5194/tc-11-427-2017, 2017.

https://doi.org/10.5194/egusphere-2024-2927
Preprint. Discussion started: 17 October 2024

Morlighem, M., Bondzio, J., Seroussi, H., Rignot, E., Larour, E., Humbert, A., and Rebuffi, S.: Modeling of Store Gletscher's calving dynamics, West Greenland, in response to ocean thermal forcing, Geophysical Research Letters, 43, 2659–2666, 2016.

Nick, F., van der Veen, C., Vieli, A., and Benn, D.: A physically based calving model applied to marine outlet glaciers and implications for the glacier dynamics, Journal of Glaciology, 56, 781–794, https://doi.org/10.3189/002214310794457344, 2010.

Nick, F. M., Vieli, A., Andersen, M. L., Joughin, I., Payne, A., Edwards, T. L., Pattyn, F., and van de Wal, R. S. W.: Future sea-level rise from Greenland's main outlet glaciers in a warming climate, Nature, 497, 235–238, https://doi.org/10.1038/nature12068, 2013.

Nye, J. F.: Comments on Dr. Loewe's letter and notes on crevasses, Journal of Glaciology, 2, 512–514, 1955.

Petlicki, M., Cieply, M., Jania, J. A., Prominska, A., and Kinnard, C.: Calving of a tidewater glacier driven by melting at the waterline, Journal of Glaciology, 61, 851–863, https://doi.org/10.3189/2015JoG15J062, 2015.

Pfeffer, W., Dyurgerov, M., Kaplan, M., Dwyer, J., Sassolas, C., Jennings, A., Raup, B., and Manley, W.: Numerical modeling of late Glacial Laurentide advance of ice across Hudson Strait: Insights into terrestrial and marine geology, mass balance, and calving flux, Paleoceanography, 12, 97–110, 1997.

Sartore, N. B., Wagner, T. J., Siegfried, M. R., Pujara, N., and Zoet, L. K.: Calving of Ross Ice Shelf from wave erosion and hydrostatic stresses, EGUsphere, 2024, 1–23, 2024.

Schlemm, T. and Levermann, A.: A simple stress-based cliff-calving law, The Cryosphere, 13, 2475–2488, https://doi.org/10.5194/tc-13-2475-2019, 2019.

Seroussi, H., Nowicki, S., Payne, A. J., Goelzer, H., Lipscomb, W. H., Abe-Ouchi, A., Agosta, C., Albrecht, T., Asay-Davis, X., Barthel, A., Calov, R., Cullather, R., Dumas, C., Galton-Fenzi, B. K., Gladstone, R., Golledge, N. R., Gregory, J. M., Greve, R., Hattermann, T., Hoffman, M. J., Humbert, A., Huybrechts, P., Jourdain, N. C., Kleiner, T., Larour, E., Leguy, G. R., Lowry, D. P., Little, C. M., Morlighem, M., Pattyn, F., Pelle, T., Price, S. F., Quiquet, A., Reese, R., Schlegel, N.-J., Shepherd, A., Simon, E., Smith, R. S., Straneo, F., Sun, S., Trusel, L. D., Van Breedam, J., van de Wal, R. S. W., Winkelmann, R., Zhao, C., Zhang, T., and Zwinger, T.: ISMIP6 Antarctica: a multi-model ensemble of the Antarctic ice sheet evolution over the 21st century, The Cryosphere, 14, 3033–3070, https://doi.org/10.5194/tc-14-3033-2020, 2020.

Slater, D. A., Benn, D. I., Cowton, T. R., Bassis, J. N., and Todd, J. A.: Calving Multiplier Effect Controlled by Melt Undercut Geometry, Journal of Geophysical Research: Earth Surface, 126, e2021JF006 191, https://doi.org/10.1029/2021JF006191, 2021.

Todd, J., Christoffersen, P., Zwinger, T., Raback, P., Chauche, N., Benn, D., Luckman, A., Ryan, J., Toberg, N., Slater, D., and Hubbard, A.: A Full-Stokes 3D Calving Model applied to a large Greenlandic Glacier, Journal of Geophysical Research: Earth Surface, 123, 410–432, https://doi.org/10.1002/2017JF004349, 2018.

Todd, J., Christoffersen, P., Zwinger, T., Råback, P., and Benn, D. I.: Sensitivity of a calving glacier to ice–ocean interactions under climate change: new insights from a 3-D full-Stokes model, The Cryosphere, 13, 1681–1694, https://doi.org/10.5194/tc-13-1681-2019, 2019.

Van der Veen, C.: Tidewater calving, Journal of Glaciology, 42, 375–385, 1996.

Van der Veen, C.: Calving glaciers, Progress in Physical Geography, 26, 96–122, 2002.

van der Veen, C. J.: Fracture mechanics approach to penetration of surface crevasses on glaciers, Cold Regions Science and Technology, 27, 31–47, https://doi.org/10.1016/S0165-232X(97)00022-0, 1998.

van Dongen, E. C. H., Åström, J. A., Jouvet, G., Todd, J., Benn, D. I., and Funk, M.: Numerical Modeling Shows Increased Fracturing Due to Melt-Undercutting Prior to Major Calving at Bowdoin Glacier, Frontiers in Earth Science, 8, 253, https://doi.org/10.3389/feart.2020.00253, 2020.

https://doi.org/10.5194/egusphere-2024-2927
Preprint. Discussion started: 17 October 2024

Wagner, T. J. W., James, T. D., Murray, T., and Vella, D.: On the role of buoyant flexure in glacier calving, Geophysical Research Letters, 43, 232–240, https://doi.org/10.1002/2015GL067247, 2016.

Wagner, T. J. W., Straneo, F., Richards, C. G., Slater, D. A., Stevens, L. A., Das, S. B., and Singh, H.: Large spatial variations in the flux balance along the front of a Greenland tidewater glacier, The Cryosphere, 13, 911–925, https://doi.org/10.5194/tc-13-911-2019, 2019.

Weertman, J.: Can a water-filled crevasse reach the bottom surface of a glacier?, in: Association Internationale d'Hydrologie Scientifique. Commission de Neiges et Glaces. Symposium on the Hydrology of Glaciers, Cambridge, 7-13 September 1969, pp. 139–45, 1973.

Wehrlé, A., Lüthi, M. P., and Vieli, A.: The control of short-term ice mélange weakening episodes on calving activity at major Greenland outlet glaciers, The Cryosphere, 17, 309–326, https://doi.org/10.5194/tc-17-309-2023, 2023.

Wilner, J. A., Morlighem, M., and Cheng, G.: Evaluation of four calving laws for Antarctic ice shelves, The Cryosphere, 17, 4889–4901, https://doi.org/10.5194/tc-17-4889-2023, 2023.

Wilson, E. A., Wells, A. J., Hewitt, I. J., and Cenedese, C.: The dynamics of a subglacial salt wedge, Journal of Fluid Mechanics, 895, A20, https://doi.org/10.1017/jfm.2020.308, 2020.

Yu, H., Rignot, E., Morlighem, M., and Seroussi, H.: Iceberg calving of Thwaites Glacier, West Antarctica: full-Stokes modeling combined with linear elastic fracture mechanics, The Cryosphere, 11, 1283–1296, 2017.

Zarrinderakht, M., Schoof, C., and Peirce, A.: The effect of hydrology and crevasse wall contact on calving, The Cryosphere, 16, 4491–4512, https://doi.org/10.5194/tc-16-4491-2022, 2022.